HHS Public Access

Author manuscript

Conf Proc IEEE Eng Med Biol Soc. Author manuscript; available in PMC 2018 January 28.

Published in final edited form as:

Conf Proc IEEE Eng Med Biol Soc. 2017 July ; 2017: 580–583. doi:10.1109/EMBC.2017.8036891.

Development of semi-automatic procedure for detection and tracking of fiducial markers for orofacial kinematics during natural feeding

Filiz Bunyak[1], **Naru Shiraishi**[2,3], **Kannappan Palaniappan**[1], **Teresa E. Lever**[4], **Limor Avivi-Arber**[5], and **Kazutaka Takahashi**[2] **[Senior Member, IEEE]**

[1]Department of Computer Science, University of Missouri, Columbia, MO 65211

[2]Division of Dysphagia Rehabilitation, Graduate School of Medical and Dental Sciences, Niigata University, Niigata, Niigata, Japan

[3]Department of Organismal Biology and Anatomy, University of Chicago, Chicago, IL 60637 USA

[4]Department of Otolaryngology-Head and Neck Surgery, University of Missouri School of Medicine, Columbia, MO 65212, USA

[5]Department of Prosthodontics, Faculty of Dentistry, University of Toronto, Toronto, ON M5G 1G6, Canada

Abstract

Feeding is a highly complex, essential behavior for survival in all species. Characterization of feeding behaviors has implications in basic science and translational medicine. We have been developing methods to study feeding behaviors using high speed videofluoroscopy (XROMM) in rats while self-feeding radiopaque flavored kibble. The rat is a popular model in translational medicine; however, it has not been studied using this methodology. Towards this goal, we surgically implanted radiopaque fiducial markers into the skull, mandible, and tongue of rats to enable motion tracking. We are developing computer vision tools to extract kinematics and behavioral features from XROMM videos to overcome barriers of current analysis methods. By understanding feeding dynamics, we will gain basic scientific knowledge and translational insights for feeding disorders caused by neurological conditions such as ALS, Parkinson's disease, and stroke.

I. INTRODUCTION

We have been developing surgical and data collection methods for using 3D high-speed videofluoroscopy (XROMM - X-ray Reconstruction of Moving Morphology [1], [2]) with rats to assess changes in feeding behaviors due to oral environmental modifications (e.g., tooth loss [3]) and neurodegenerative conditions such as Parkinson's disease. Feeding is a highly complex, life-sustaining behavior that is effortlessly orchestrated by multiple cortical and subcortical structures to integrate reflexive and voluntary movements that seamlessly intercalate several behaviorally characterized stages: ingestion, manipulation, stage 1 transport, rhythmic chewing, stage 2 transport, and swallowing of food and liquid boluses [4]. Using XROMM methods, feeding behaviors have been studied by tracking radiopaque

fiducial markers that are surgically implanted into bony and soft tissue craniofacial structures of several animal species, including turkeys, carp, and pigs [1], [2]. However, XROMM methodology has not yet been established for use with rats, a popular species in translational medicine. Moreover, one of the major bottlenecks to process XROMM data (regardless of species) to study feeding behaviors is a lack of established methods for feature tracking of radiopaque markers. Currently, massive amounts of manual digitization must be performed to process XROMM data to just extract marker kinematics, and few efforts have been made to make the digitization process more efficient or automated [5]–[7]. Thus, there remains a critical need to develop XROMM image processing tools for high throughput detection and tracking of markers during mammalian feeding to hasten the scientific discovery process.

Tracking and extraction of relevant behavioral parameters remains to be a challenging task due to 1) unconstrained movements of rats during feeding, 2) obstruction of the marker implants by the oral contrast agent required for radiographic visualization of bolus flow, 3) change in location of the anatomical markers and the bony structures from CT data during longitudinal studies as animals grow and during serial CT sessions requiring anesthesia and radiation, 4) indistinct appearances of markers, and 5) detection errors such as over- and under-segmentations. Furthermore, unlike other XROMM studies, we are preparing to perform group studies for which we have multiple animals per group and data collection takes place daily over several weeks. Despite the presence of integrated software to process XROMM data (XMA lab, http://www.xromm.org/xmalab), it is still heavily GUI based and is not suited to process massive amounts of data semiautomatically. Thus, we aim to develop methods to efficiently track fiducial markers during unconstrained feeding and to characterize behavioral states from XROMM videos of rats. Our image processing and computer vision pipeline used for persistent tracking of radiopaque markers and other bony landmarks consists of three main modules: fiducial marker detection, marker tracking, and track management.

II. METHODS

A. Experimental Procedure and Behavioral Task

All surgical procedures and experimental protocols were approved by the University of Chicago Institutional Animal Care and Use Committee. Under isoflurane anesthesia, Sprague-Dawley rats (n=8, 12 weeks or older, over 250 g, both females and males) were immobilized in a stereotaxic frame for implantation of sterilized tantalum bead fiducial markers (0.5 mm diameter; Baltec, Los Angeles, CA) with a 21 gauge hypodermic needle. Twelve markers were implanted into bony structures (4 into the top of the skull and 4 into each side of the mandible) after drilling depressions in the bone, and 7 markers were implanted into the tongue (3 anterior, 3 middle, and 1 posterior) (Fig. 1). After recovery from surgery, the animals were acclimated to eating radiopaque food (barium-extruded kibble with peanut flavoring: AFB International, St. Charles, MO) while placed in an experimental chamber up to 1 hour per day, twice a week.

B. Fiducial Marker Detection

In order to track motion of the skull, mandible, and tongue of animals, radiopaque markers were surgically implanted and imaged using high speed biplanar videofluoroscopy (XROMM). The tracking was performed on images obtained by one camera at a time. We use Laplacian of Gaussian (LoG) blob detection to locate the implanted markers:

$$\nabla^2 L = L_{xx} + L_{yy}$$
$$L(x, y, \sigma) = g(x, y, \sigma) * I(x, y) \quad (1)$$

where $I(x, y)$ is the original image and $g(x, y, \sigma)$ is a Gaussian kernel with scale σ. LoG output is processed with morphological h-maxima operation to suppress local maxima whose height is lower than a threshold. LoG is more robust to image contrast and intensity variations compared to raw intensity values and detects prominent dark blobs (markers) while limiting spurious detections as in [8], [9].

C. Tracking Multiple Interacting Markers

To track multiple interacting markers, we have developed a probabilistic multi-object tracking system with an explicit split, merge, and occlusion handling module. This is an extension of our earlier cell and bacteria tracking works [10], [11]. The proposed tracking system uses a probabilistic graph-based frame to frame correspondence analysis module with the following major steps: (1) match probability computation, (2) absolute match pruning, (3) bi-directional (forward-backward) relative match pruning, and (4) match classification. Match probabilities between detected markers in $frame(t-1)$ and detected markers in $frame(t)$ are computed and stored in an $n_{t-1} \times n_t$ matrix P, where n_{t-1} and n_t are the number of detected markers in $frame(t-1)$ and $frame(t)$, respectively. Match probability for a pair of marker positions $p_i(t-1)$ and $q_j(t)$ is computed as:

$$P(p_i, q_j) = exp\left(-\frac{\|p_i - q_j\|}{\sigma}\right) \quad (2)$$

An additional $n_{t-1} \times n_t$ binary match matrix M is formed and initially set to 1. Frame to frame correspondences are determined after absolute and relative match pruning.

Absolute pruning—Matches whose probabilities are lower than a minimum probability value P_{min} are pruned by setting corresponding elements in M to 0:

$$P(p_i, q_j) < P_{min} \Rightarrow M(p_i, q_j) = 0 \quad p_i \in 1..n_{t-1}, q_j \in 1..n_t \quad (3)$$

Forward relative pruning—For each detected marker $p_i(t-1)$, the best matching marker $q^*(t)$ is determined. Matches for $p_i(t-1)$, whose probabilities are lower than $T_R \times P(p_i, q^*)$, where T_R is a constant, are pruned:

$$P(p_i, q_j) < T_R \times P(p_i, q^*) \Rightarrow M(p_i, q_j) = 0 \quad p_i \in 1..n_{t-1}, q_j \in 1..n_t \quad (4)$$

Backward relative pruning—For each detected marker $q_j(t)$, the best matching marker $p^*(t-1)$ is determined. Matches for $q_j(t)$, whose probabilities are lower than $T_R \times P(p^*, q_j)$ are pruned:

$$P(p_i, q_j) < T_R \times P(p^*, q_j) \Rightarrow M(p_i, q_j) = 0 \quad p_i \in 1..n_{t-1}, q_j \in 1..n_t \quad (5)$$

A multi-frame correspondence graph $\mathcal{G}$ is formed, where nodes represent marker instances and edges represent correspondences. Using match matrix M, frame to frame correspondences are determined and markers are linked in time. The described scheme supports one-to-one, many-to-one, one-to-many, one-to-none, and none-to-one matches corresponding to track extension, merge, split, termination, and initialization, respectively. Tracks are formed by traversing the edges of $\mathcal{G}$. A multi-hypothesis testing approach is used for longer term data association.

D. Track Management

The track management module resolves correspondence ambiguities, filters spurious tracks, and handles occlusions and merge/split cases. The module incorporates context sensitive information to resolve spatiotemporal ambiguities or to correct false detections and/or false associations. The types of information used include velocity, neighborhood, and common motion constraints, set according to the characteristics of the host structure (markers on rigid jaw versus deformable tongue). Some marker to marker interaction patterns are illustrated in Figure 2. While simple best-match data association can handle case a, cases b–d require split-merge analysis in order to preserve accurate marker/track identities in time. Although markers cannot split, merge, appear, or disappear because of segmentation errors or occlusions, the tracks may appear to do so. In order to maintain correct track identity, these events must be resolved. False merge/split events may be caused by different scenarios requiring different refinement actions. Figure 3 illustrates a track split-merge event and corresponding corrective actions. The track management module uses information listed above and Kalman state estimation to resolve these tracking ambiguities. Tracked videos from both cameras can be brought back into XMA lab to obtain 3D positions of the markers. We are in the process of incorporating a second camera output to better diagnose and correct these detection and matching problems before calculating 3D positions of the markers.

III. Experimental Results

Figure 4 shows sample fiducial marker detection results for three different poses on the same video sequence. The animal contains 19 fiducial markers (4 on the skull, 4 on each side of the mandible, and 7 on the tongue). Figure 4a shows 18 detections (17 correct, 1 merge/partial occlusion). Figure 4b shows 19 detections (all correct). Figure 4c shows 19 detections (1 not visible, 1 false positive).

Figure 5 illustrates fiducial marker tracking results on a sample sequence. The tracks are visualized in 2D over the last frame and as a 3D plot, where z axis denotes time.

IV. Conclusion and Future Works

We have developed a set of algorithms to semi-automatically detect and track fiducial markers in single plane XROMM data of unconstrained rat feeding. We are planning to extend the present work to develop pattern recognition and machine learning tools not only to mine trajectory data, but also to represent, recognize, and analyze higher-level motion patterns linked to feeding behaviors, particularly to classify entire feeding sequences into cycle types such as ingestion, manipulation, chewing, and swallowing as well as phases within each gape cycle which are often divided into four phases: slow opening (SO), slow closing (SC), fast opening (FO), and fast closing (FC) [4]. Furthermore, if massive amounts of 3D feeding data, especially totally unconstrained motions, can be processed with unprecedented efficiency, then studying interactions of orofacial effectors can be described. Our preliminary results to apply the similar algorithms to detect landmarks as opposed to markers to capture jaw and incisor displacements have been successfully applied to mouse drinking behavior for multiple jaw cycles (Fig. 6).

By combining electrophysiological signals with high fidelity kinematics during feeding, a new opportunity will be open to study neural processes of orofacial apparatus motor control as it has been done in other types of complex movements such as 3D reach-to-grasp kinematics [12], [13]. Such knowledge will enhance our understanding of the neural control of feeding behaviors in conditions of health and disease.

Acknowledgments

The authors would like to thank Nicholas Gidmark for assistance with the XROMM set up and the veterinary staff of the animal research center (ARC) at the University of Chicago for animal care and surgical procedures.

K.T. was supported by NIH R01 DE023816. N.S. was supported by Strategic Young Researcher Overseas Visits Program for Accelerating Brain Circulation, JSPS, JAPAN. This work was supported by National Center for Advancing Translational Sciences of the National Institutes of Health through Grant Number UL1 TR000430 and Mizzou advantage funding.

References

1. Brainerd, Elizabeth L., Baier, David B., Gatesy, Stephen M., Hedrick, Tyson L., Metzger, Keith a, Gilbert, Susannah L., Crisco, Joseph J. X-ray reconstruction of moving morphology (XROMM): precision, accuracy and applications in comparative biomechanics research. Journal of experimental zoology Part A, Ecological genetics and physiology. 2010; 313(5):262–279.
2. Gidmark NJ, Staab KL, Brainerd EL, Hernandez LP. Flexibility in starting posture drives flexibility in kinematic behavior of the kinethmoid-mediated premaxillary protrusion mechanism in a cyprinid fish, Cyprinus carpio. Journal of Experimental Biology. 2012; 215(13):2262–2272. [PubMed: 22675187]
3. Shiraishi, N., Avivi-Arber, L., Lever, T., Inoue, M., Ross, C., Takahashi, K. Development Of A Rat Model For Studying The Relationship Between Oral Environmental Changes And Alterations In Mastication/Swallowing Patterns. Dysphagia research society annual meeting; Portland, OR. 2017.
4. Thexton AJ, Hiiemae KM, Crompton AW. Food consistency and bite size as regulators of jaw movement during feeding in the cat. J Neurophysiol. 1980; 44(3):456–474. [PubMed: 7441310]

5. Best, Matthew D., Nakamura, Yuki, Kijak, Nicoletta A., Allen, Mitchell J., Lever, Teresa E., Hatsopoulos, Nicholas G., Ross, Callum F., Takahashi, Kazutaka. Semiautomatic marker tracking of tongue positions captured by videofluoroscopy during primate feeding. Proceedings of the Annual International Conference of the IEEE Engineering in Medicine and Biology Society, EMBS; 2015; 2015 Novem. p. 5347-5350.

6. Lam, Shing Chun Benny, McCane, Brendan, Allen, Robert. Automated tracking in digitized videofluoroscopy sequences for spine kinematic analysis. Image Vision Comput. Sep; 2009 27(10): 1555–1571.

7. Zheng Y, Nixon MS, Allen R. Lumbar spine visualisation based on kinematic analysis from videofluoroscopic imaging. Medical Engineering & Physics. 2003; 25(3):171–179. 3-D Computer Visualization and Animation of Medical Images. [PubMed: 12589715]

8. Sun M, Huang J, Bunyak F, Gumpper K, De G, Sermersheim M, Liu G, Lin P-H, Palaniappan K, Ma J. Superresolution microscope image reconstruction by spatiotemporal object decomposition and association: application in resolving t-tubule structure in skeletal muscle. Optics Express. May; 2014 22(10):12160–12176. [PubMed: 24921337]

9. Gronkiewicz KM, Giuliano EA, Kuroki K, Bunyak F, Sharma A, Teixeira LBC, Hamm CW, Mohan RR. Development of a novel in vivo corneal fibrosis model in the dog. Experimental eye research. 2016; 143:75–88. [PubMed: 26450656]

10. Bunyak, F., Palaniappan, K., Nath, SK., Baskin, TI., Dong, G. Quantitative cell motility for in vitro wound healing using level set-based active contour tracking. IEEE Int. Symposium on Biomedical Imaging (ISBI); Apr 2006; p. 1040-1043.

11. Thutupalli S, Sun M, Bunyak F, Palaniappan K, Shaevitz JW. Directional reversals enable myxococcus xanthus cells to produce collective one-dimensional streams during fruiting-body formation. Journal of The Royal Society Interface. 2015; 12(109)

12. Saleh, Maryam, Takahashi, Kazutaka, Hatsopoulos, Nicholas G. Encoding of coordinated reach and grasp trajectories in primary motor cortex. The Journal of neuroscience : the official journal of the Society for Neuroscience. Jan; 2012 32(4):1220–32. [PubMed: 22279207]

13. Takahashi, Kazutaka, Best, Matthew D., Huh, Noah, Brown, Kevin A., Tobaa, Adil A., Hatsopoulos, Nicholas G. Encoding of both reaching and grasping kinematics in dorsal and ventral premotor cortices. Journal of Neuroscience. 2017; 37(7):1537–16.

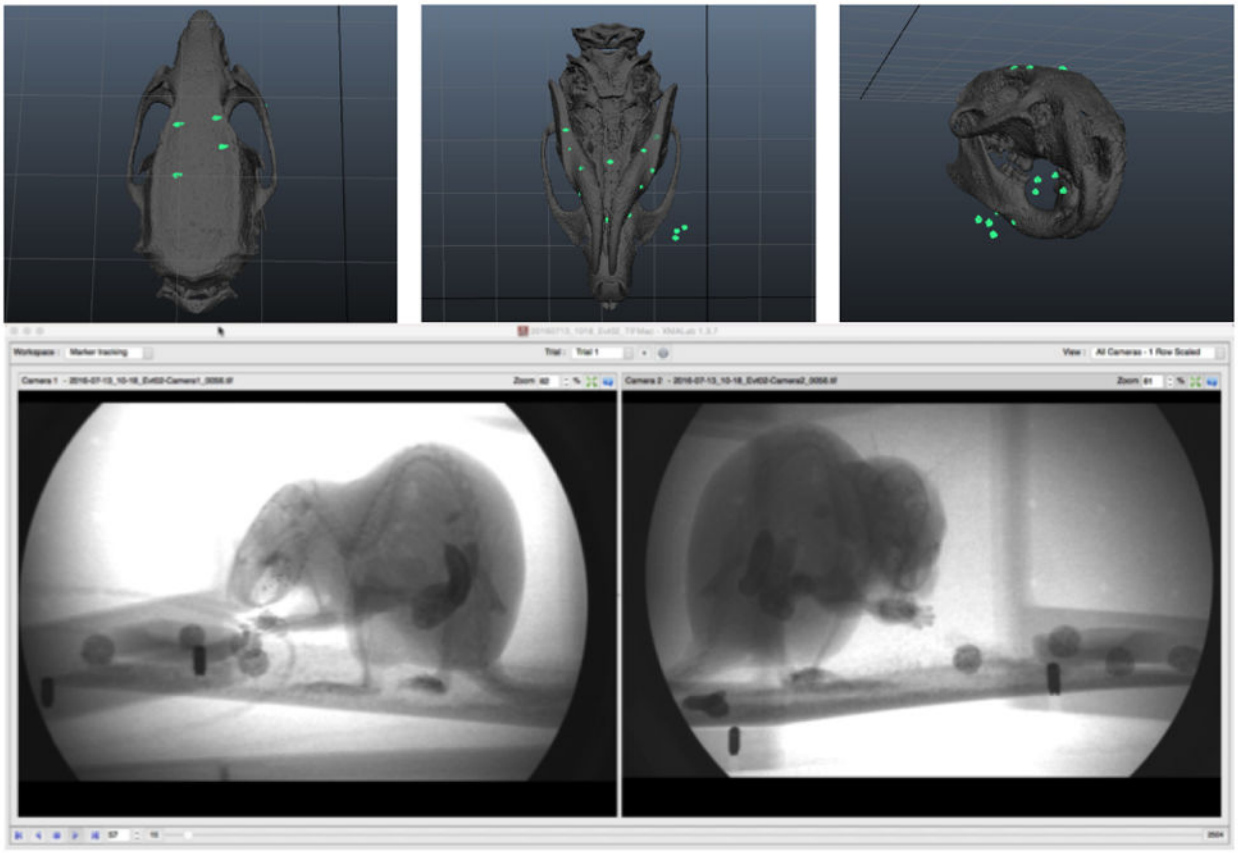

Fig. 1.

Top: Marker locations via CT scans. 4 markers on the skull (Left), 4 markers on each side of mandible (Middle), and 3 in anterior, 3 in middle, and 1 in posterior portion of the tongue (Middle and Right). Bottom: Calibrated and undistorted XROMM data during a feeding session.

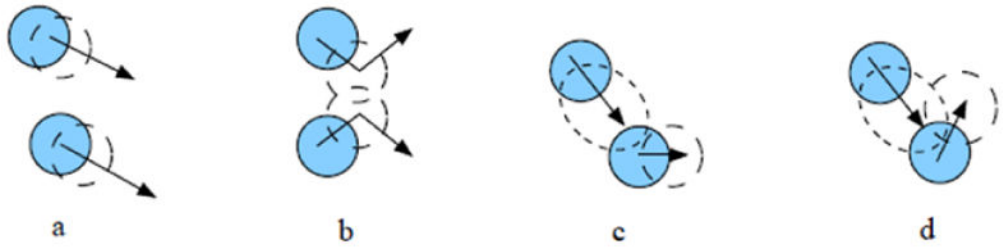

Fig. 2.

Some marker to marker interaction patterns. Filled blue current shape&location (t), dashed lines future shape & location (t+1).

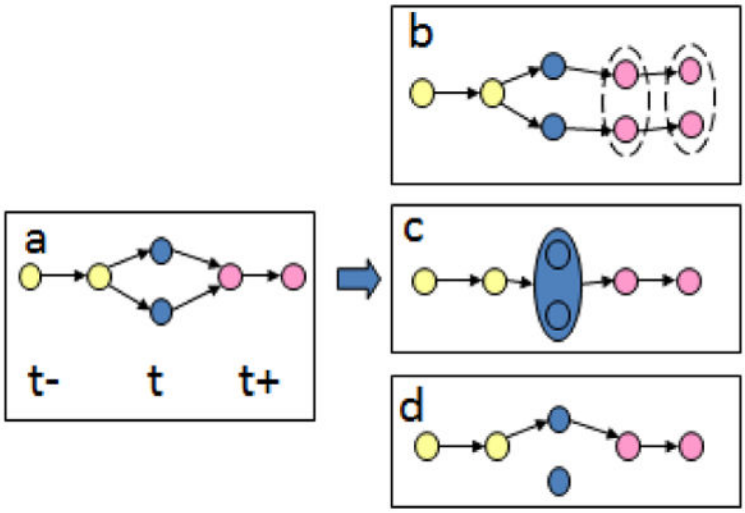

Fig. 3.

A track split-merge event (a) and three potential corrective actions (b)–(d). Yellow, blue, and, pink nodes represent past, present, and future marker instances. (b) Falsely merged markers at time *t*+ are split, (c) temporary fragmentation of a single marker at time *t* is resolved by merging the fragments, (d) link to the false-detection at time *t* is removed.

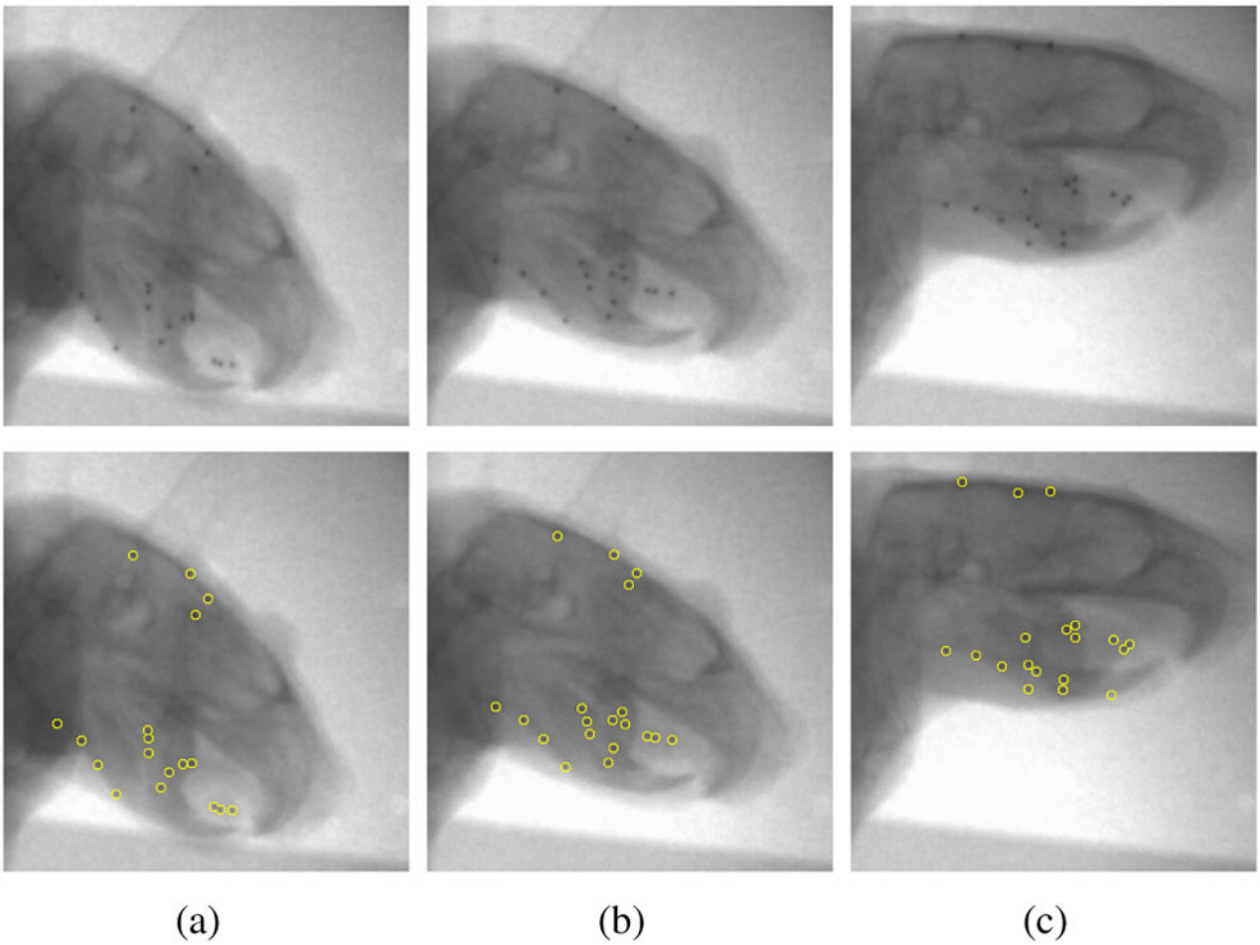

Fig. 4.
Marker detection results.

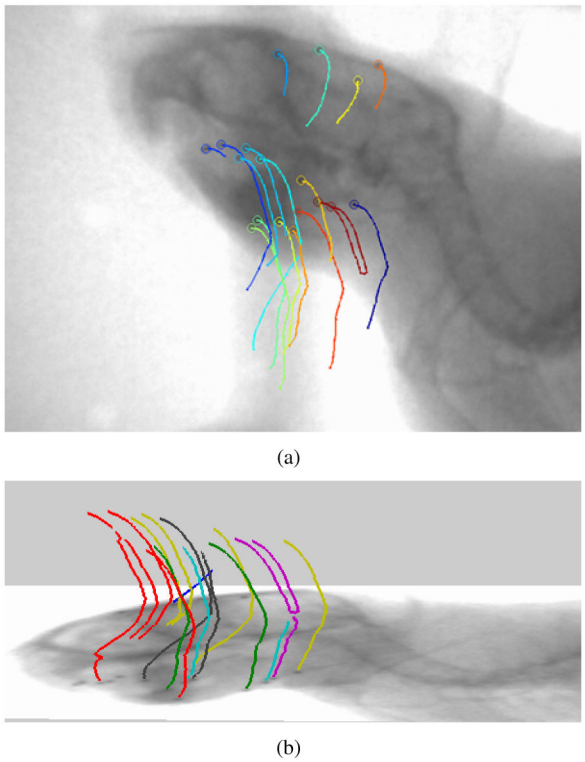

Fig. 5.
Sample fiducial marker tracking results, (a) 2D and (b) 3D visualization.

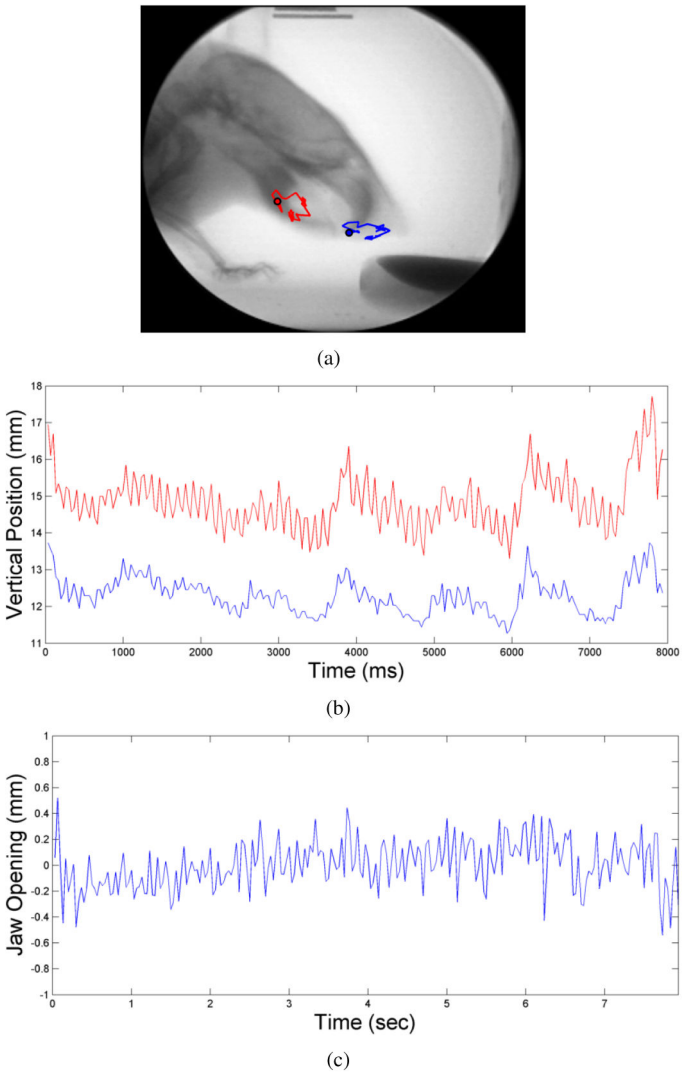

Fig. 6.

Landmark tracking results. (a) Tracks, (b) vertical motion of lower (red) and upper (blue) jaw, (c) jaw distance in time.